Quantum Monte Carlo Calculations of Structural Properties of FeO Under Pressure

Jindřich Kolorenč* and Lubos Mitas

Department of Physics and CHiPS, North Carolina State University, Raleigh, North Carolina 27695, USA

(Received 31 December 2007; published 28 October 2008)

We determine the equation of state of stoichiometric FeO by employing the diffusion Monte Carlo method. The fermionic nodes are fixed by a single Slater determinant of spin-unrestricted orbitals. The calculated ambient-pressure properties (lattice constant, bulk modulus, and cohesive energy) agree very well with available experimental data. At approximately 65 GPa, the atomic lattice changes from the rocksalt B1 to the NiAs-type inverse B8 structure.

DOI: 10.1103/PhysRevLett.101.185502 PACS numbers: 61.50.Ks, 64.30.−t, 71.15.−m, 71.20.−b

Transition metal oxides are solids with strong electron-electron correlations that lead to a rich variety of observed structural and electronic phases. These materials pose difficulties for condensed matter theories due to competitive interplay among correlation and exchange in d subshells, crystal field effects, d-p hybridization, and charge transfer. In particular, FeO represents one of the challenging simple oxides due to the nominally open-shell occupation of the $3d$ levels. High-pressure properties of FeO are of interest also in geophysics, since FeO is an end member of an important constituent of Earth's interior, $Fe_{1-x}Mg_xO$. Iron oxide proved to be problematic for the density functional theory (DFT) in the local density and generalized gradient approximations (LDA and GGA). For example, both LDA and GGA predict an incorrect ground state lattice structure [1–3].

At ambient conditions, FeO crystallizes in the B1 (NaCl-type) structure. It is antiferromagnetically ordered at temperatures below 198 K and this ordering is accompanied by a small rhombohedral distortion denoted as rB1—the unit cell is stretched along the [111] body diagonal. Shock-wave studies showed that around 70 GPa the oxide transforms to a different structure [4], which was inferred as B2 (CsCl type) in analogy with similar materials, but LDA calculations hinted that much larger pressure, around 500 GPa, would be needed to stabilize B2 against the B1 phase [5]. Besides that, no such structural transition was detected in static compression experiments [6], unless the material was significantly heated up [7]. X-ray diffraction performed along the high-temperature static compression revealed that the high-pressure structure is actually B8 (NiAs type) [7].

There are two distinct ways of putting FeO on NiAs lattice, the so-called normal B8, where iron occupies Ni sites, and inverse B8 (iB8 for short), where iron sits on As sites. It is the latter configuration that band-structure theories identify as the most stable one [1–3]. A reinterpretation of the data from Ref. [7] suggests that the high-pressure phase is a mixture of the B8 and iB8 phases [1]. On the theoretical side, the iB8 structure proved to be difficult for the LDA and GGA methods, since they predict the iB8 phase more stable not only than B8 but also than B1 at all pressures, clearly contradicting experimental findings. It has been demonstrated that inclusion of Coulomb U alleviates this problem [2,3].

In this Letter, we calculate the equation of state of stoichiometric FeO using the fixed-node diffusion Monte Carlo (DMC) method [8], a many-body computational approach that accurately treats even strongly correlated systems. For the sake of comparison with the aforementioned studies, we focus only on the two key structures—B1 with the type-II antiferromagnetic (AFM) ordering (space group $R\bar{3}m$) and iB8 also in the AFM state (group $P\bar{6}m2$). We show that the DMC method, even in its simplest version based on a single-determinant Slater-Jastrow wave function, provides a very consistent picture of this complicated system that closely follows experimental data.

The guiding wave function that determines the fermionic nodes in our DMC simulations is of the Slater-Jastrow type $\Psi_G = \Psi_S \exp[J]$, where

$$\Psi_S(\mathbf{r}_1, \ldots, \mathbf{r}_N) = \det\{\psi_\sigma\} = \det\{\phi^\uparrow_\alpha\} \det\{\phi^\downarrow_\beta\}, \quad (1a)$$

$$J(\mathbf{r}_1, \ldots, \mathbf{r}_N) = \sum_{i,j} f(\mathbf{r}_i - \mathbf{r}_j) + \sum_{i,I} g(\mathbf{r}_i - \mathbf{R}_I). \quad (1b)$$

The lowercase indices in Eq. (1b) run over electrons, the uppercase index denotes ions. The Jastrow correlation factor J contains one- and two-body terms, g and f, that have the same form as in Ref. [9] and include 17 variational parameters that were optimized within the variational Monte Carlo framework. The single determinant of spin orbitals ψ_σ becomes a product of spin-up and spin-down determinants of spatial orbitals $\{\phi^\uparrow_\alpha, \phi^\downarrow_\beta\}$ after fixing the electron spins, $N^\uparrow = N^\downarrow = N/2$, while the overall state is a spin-unrestricted antiferromagnet.

The large energy scale of core electrons poses a difficulty for DMC calculations in an analogous way as it does for plane-wave based electronic structure techniques. Therefore, we replace the atomic cores by norm-conserving pseudopotentials [10] within the so-called localization approximation [11]. We employ small-core

pseudopotentials to minimize biases caused by elimination of the core states. Recently, we have argued [12] that in transition metal compounds even small-core pseudopotentials could lead to imprecisions in describing phenomena which involve spin-related transitions. However, this should not affect the present calculations, since iron atoms in FeO stay in a high-spin state in the whole range of pressures we study in both B1 and iB8 phases. This applies to the DMC results as well as to the flavors of DFT we used to construct the Slater determinants (see Ref. [10] for details).

The quality of the fixed-node DMC total energy is determined solely by the quality of fermionic nodes of the guiding wave function. The fermionic nodes of a wave function given by Eq. (1) are controlled by the one-electron orbitals $\{\phi_\alpha, \phi_\beta\}$. Currently, the direct variational Monte Carlo optimization of such orbital sets is impractical for simulation sizes required for our study. Instead, we use one-electron orbitals from spin-unrestricted calculations with the hybrid PBE0 functional given as [13]

$$E_{xc}^{\mathrm{PBE0}} = aE_x^{\mathrm{HF}} + (1-a)E_x^{\mathrm{PBE}} + E_c^{\mathrm{PBE}}. \tag{2}$$

Here E_x^{PBE} and E_c^{PBE} are exchange and correlation parts of the PBE GGA [14], E_x^{HF} is the exact exchange from Hartree-Fock (HF) theory, and the weight a is in the range $0 < a < 1$. We have found that inclusion of the exact-exchange term into the PBE GGA has similar effect as U in the LDA + U method. The hybrid functional opens a gap in the electronic spectrum of the AFM B1 phase and stabilizes it relative to the iB8 structure. Both the gap and the transition pressure increase with increasing a. The iB8 phase is still more stable than B1 at all pressures for the mixing weight $a = 0.05$, while the transition from B1 to iB8 occurs at 5 GPa for $a = 0.1$ and at 43 GPa for $a = 0.2$. Note that in MnO, which exhibits similar structural transition, the experimental range of transition pressures is reached already for $a \approx 0.1$ [12], whereas in the present case of FeO, the transition takes place much sooner than in experiments ($\geq$70 GPa) even for twice as large exact-exchange weight in the PBE0.

The exchange-correlation functional of Eq. (2) defines a one-parametric class of single-particle orbitals $\{\phi_\alpha^{(a)}, \phi_\beta^{(a)}\}$, which can be used to minimize the DMC fixed-node error by varying the exact-exchange weight a. Although in simple insulators, such as silicon, the differences between fixed-node energies corresponding to various sets of one-particle states were found to be rather marginal [15], more pronounced differences have been observed for transition metal systems. In isolated transition metal monoxide molecules, the fixed-node DMC energies with orbitals from the B3LYP (a hybrid functional similar to the PBE0) are noticeably lower than with the HF or pure DFT orbitals [9,16]. DMC optimization of the exact-exchange proportion in the B3LYP was performed in Ref. [16] for MnO molecule. The optimal value was reported as approximately 17%, but the minimum was rather broad and shallow and values between 5% and 30% were almost equivalent. Therefore, we have chosen the weight a in the PBE0 to be $a = 0.2$; i.e., 20% of the GGA exchange is replaced with the exact exchange. In the following we abbreviate this functional as $\mathrm{PBE0}_{20}$. This choice is compatible with findings of Ref. [16] and leads to reasonable ambient-pressure properties of FeO already within the (hybrid) DFT; i.e., the B1 structure is insulating and more stable than iB8. We have also checked that at equilibrium the $\mathrm{PBE0}_{20}$ orbitals provide lower DMC energy than either pure HF or pure PBE GGA. For example, the energy gain associated with the $\mathrm{PBE0}_{20}$ orbitals was $\approx$0.3 eV/FeO when compared to the HF orbitals.

We represent the infinite crystal by a periodically repeated simulation cell containing 8 FeO units, i.e., 176 valence and semicore electrons. Although such a system is certainly not small to deal with in an explicitly many-body fashion, finite-size errors turn out to be significant if not treated properly. The origin of these errors is twofold. One part is related to incorrect momentum quantization due to confinement of electrons into the simulation cell, the second part comes from the artificial periodicity of the exchange-correlation hole introduced by Ewald sum.

In order to eliminate the first part of the bias, we average over the so-called twisted boundary conditions. This type of average is closely related to momentum integration over the first Brillouin zone in mean-field band theories [17]. In this study we deal only with insulating states and we have found that just 8 twists are enough for our simulation cell size. We have verified that within the $\mathrm{PBE0}_{20}$ the total energy obtained in our simulation cell using 8 $\mathbf{k}$ points differs only $\approx$ 0.01 eV/FeO from fully converged integral over the Brillouin zone.

The second part of the finite-size errors is accounted for by the correction introduced in Ref. [18] where the energy at infinite volume is written as

$$E = E_{\mathrm{Ewald}} + \frac{1}{4\pi^2}\int_D d^3k \frac{S(\mathbf{k})}{k^2}. \tag{3}$$

The static structure factor is defined as $S(\mathbf{k}) = \langle\Psi_0|\hat{\rho}_{\mathbf{k}}\hat{\rho}_{-\mathbf{k}}|\Psi_0\rangle/N$ with $\hat{\rho}_{\mathbf{k}}$ standing for a Fourier component of the electron density. The integral in Eq. (3) runs over a domain D centered around $\mathbf{k} = 0$ and having volume $8\pi^3/\Omega$, where Ω is volume of the simulation cell. The structure factor $S(\mathbf{k})$ is evaluated within the DMC method at a discrete set of points and then extrapolated towards $\mathbf{k} = 0$. Performance of Eq. (3) applied to FeO is illustrated in Fig. 1, where we plot the total energy at two different electron densities as calculated in simulation cells of varied size up to 16 FeO units, i.e., 352 valence and semicore electrons. The correction eliminates more than 90% of the finite-size bias and enables us to replace the expensive size scaling analysis of Fig. 1 by a simple formula, Eq. (3).

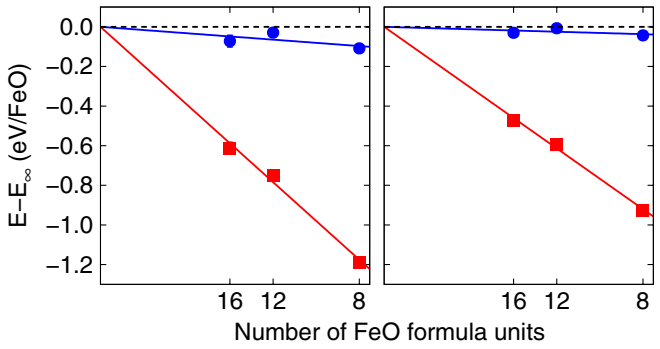

FIG. 1 (color online). Finite-size errors of the twist averaged DMC energy at volumes 15.9 Å^3/FeO (left) and 20.4 Å^3/FeO (right). Shown are Ewald energies (red squares) and values corrected by Eq. (3) (blue circles). The finite-size errors increase with increasing electron density. The residual bias of the corrected data also grows, the rate is ≈ 0.015 eV Å^{-3}/FeO. The energy in the infinite cell E_∞ is extrapolated from the data shown. Statistical error bars are smaller than the symbol sizes (here, as well as in Fig. 2).

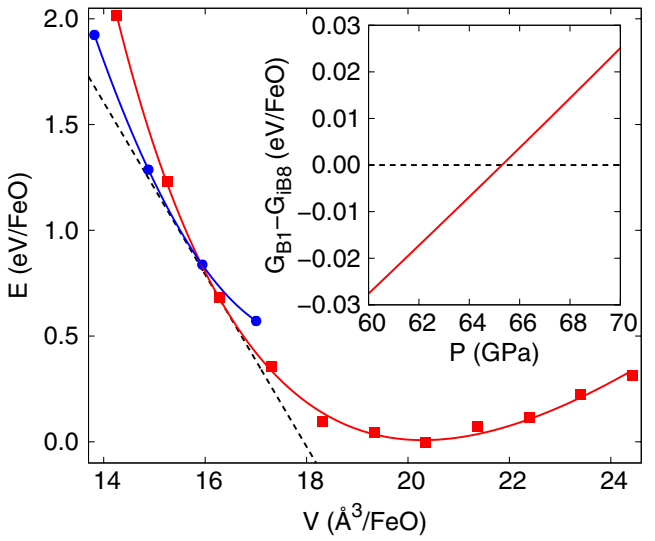

FIG. 2 (color online). Total energies of the B1 (red squares) and the iB8 (blue circles) phases. Lines are fits with Murnaghan equation of state. Inset: Difference between Gibbs potentials of the two phases at $T = 0$ K.

Results.—Let us first discuss equilibrium properties of the B1 phase. For the cohesion energy, $E_{\rm coh} = E_{\rm Fe} + E_{\rm O} - E_{\rm FeO}$, our DMC simulations yield 9.66 ± 0.04 eV/FeO that matches 9.7 eV/FeO deduced from experimental formation enthalpies [19]. The electronic gap, estimated as a difference between total energies of the ground and the first excited states at the Γ point of our 8 FeO simulation cell, comes out as 2.8 ± 0.3 eV. This value is not too far from the optical absorption edge observed near 2.4 eV [20]. The weak feature displayed between 1.0 and 1.5 eV in these experiments is not reproduced in the theoretical picture of FeO we present here. This feature is possibly related to imperfections in structural or magnetic order, since essentially the same absorption band was repeatedly observed in other systems where Fe atoms act as impurities [21,22].

The DMC energy is plotted as a function of volume in Fig. 2 together with fitted Murnaghan equation of state. An alternative fit with Vinet equation of state provides virtually identical results (see Ref. [10]). The parameters of the least-squares fit are compared with other electronic structure methods and with experiments in Table I. The DMC estimate for the equilibrium lattice constant a_0 is in excellent agreement with experimental value extrapolated to the stoichiometric FeO and offers more consistent prediction than the LDA or GGA. All methods shown in Table I provide essentially the same value of the bulk modulus K_0 that is noticeably larger than typical experimental results. However, extrapolation to stoichiometry leads to values in the vicinity of the theoretical data [23–25]. The isothermal pressure derivative of the bulk modulus K_0' turns out to be larger in the DMC method than in the DFT. The DMC prediction is compatible with elastic-wave experiments [24].

We impose the cubic symmetry for the low-pressure B1 phase; i.e., the rhombohedral distortion is neglected. We have checked the impact of this restriction by comparing DMC total energies for different distortions at high compression, where the distortion is enhanced. At the volume of 15.3 Å^3/FeO, the energy gain associated with the rhombohedral distortion was of the order of statistical error bars ≈ 0.02 eV/FeO, i.e., too small to affect the results (at least within the DMC method with a single-determinant guiding wave function).

In the high-pressure iB8 phase, the c/a ratio has been optimized within the PBE0$_{20}$. We have found an increase from 1.93 at volume 17 Å^3/FeO to 2.03 at 14 Å^3/FeO. These ratios agree well with experimental $c/a = 2.01$ at 14.83 Å^3/FeO reported in Ref. [7].

The pressure $P_c = 65 \pm 5$ GPa of the structural transition from the B1 to the iB8 phase has been determined from equality of Gibbs potentials, $G_{\rm B1}(P_c) = G_{i\rm B8}(P_c)$; see Fig. 2. The error bar is given by statistical uncertainties of the Monte Carlo data. A correction for the residual

TABLE I. Equilibrium lattice constant a_0, bulk modulus K_0, and its derivative $K_0' = (\partial K_0/\partial P)_T$ calculated in this work (DMC and PBE0$_{20}$, $T = 0$ K) compared to selected theories and room-temperature experiments. The experimental a_0 is extrapolated to the stoichiometric FeO, the experimental K_0 and K_0' correspond to Fe$_{0.943}$O.

	a_0 (Å)	K_0 (GPa)	K_0'
DMC	4.324(6)	170(10)	5.3(7)
PBE0$_{20}$	4.328	182	3.7
GGA [3]	4.28	180	3.6
LDA [5]	4.136	173	4.2
Experiment	4.334 [23]	152.3 [24]	4.92 [24]

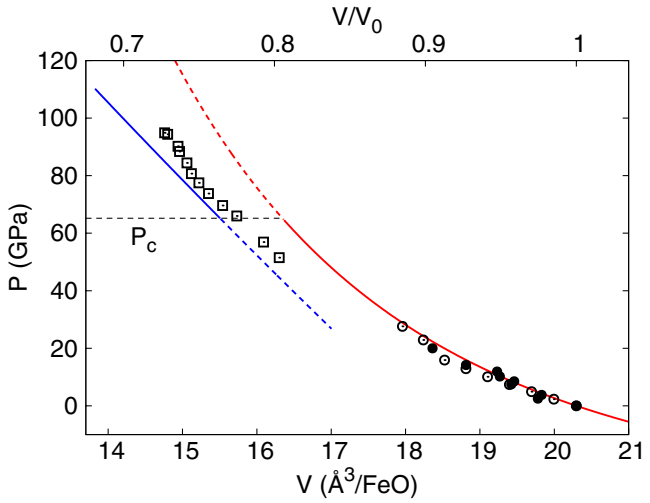

FIG. 3 (color online). $P(V)$ curves of the B1 (red, low pressure) and the iB8 (blue, high pressure) phases. Lines are our DMC fits as in Fig. 2. Points are experimental data: filled circles [6] (B1, $Fe_{0.98}O$), empty circles [28] (B1, $Fe_{0.94}O$), empty squares [7] (iB8, $Fe_{0.98}O$). All B1 data [6,28] were taken at room temperature, the iB8 data [7] at 900 K. B1 data sets are shown relative to the equilibrium volume to reduce the nonstoichiometry effects.

finite-size error quoted in Fig. 1 would raise this pressure by less than 3 GPa. Our estimate corresponds to low temperatures, where experiments suggest considerably higher transition pressure P_c. It was proposed that an energy barrier requiring a thermal activation could cause a seemingly elevated P_c [6,26]. In such a scenario, the iB8 phase should be stable at low temperatures once it is produced. Recent experiments show that iB8 is quenchable down to room temperatures, but instabilities occur under a subsequent pressure decrease [27].

Another mechanism that could alter the relative stability of the B1 and the iB8 phases is the presence of defects and nonstoichiometry. A reduced stability of the iB8 phase associated with departure from the ideal FeO lattice can be deduced from experiments on closely related materials. In $Fe_{1-x}O$, iB8 is less stable than theory suggests for clean FeO, and no iB8 is observed in Fe_{1-x} Mg_xO even with as little as 5% of Mg in the sample [27].

Additional means of comparison of our data with experiments is the $P(V)$ equation of state, Fig. 3. Agreement between data for the B1 structure (after extrapolation to stoichiometric FeO) is very good and reaffirms similarly close correspondence of ambient-pressure parameters shown in Table I. Our curve for the iB8 structure also follows the x-ray data of Ref. [7] rather nicely (no stoichiometry related correction was attempted in this case).

In summary, the equation of state and basic electronic structure of FeO calculated with the diffusion Monte Carlo method agrees very well with many aspects of available experimental data. Considering that the DMC calculations are essentially parameter-free and that the fixed-node condition was enforced using a single Slater determinant wave function, the degree of consistency of the provided picture is quite remarkable.

We acknowledge support by NSF EAR-0530110 and DOE DE-FG05-08OR23336 grants. This study was enabled by INCITE and CNMS allocations at ORNL and by allocation at NCSA. Quantum Monte Carlo simulations were done using QWALK code [29], the one-particle orbitals were calculated with CRYSTAL2003 [30]. The Gaussian basis set was saturated to match the CRYSTAL2003/LDA equation of state with corresponding calculations utilizing linearized augmented plane waves, analogously to Ref. [12].

*On leave from: Institute of Physics, Academy of Sciences of the Czech Republic, Na Slovance 2, CZ-18221 Praha 8, Czech Republic.
kolorenc@fzu.cz

[1] I. I. Mazin *et al.*, Am. Mineral. **83**, 451 (1998).
[2] Z. Fang *et al.*, Phys. Rev. Lett. **81**, 1027 (1998).
[3] Z. Fang *et al.*, Phys. Rev. B **59**, 762 (1999).
[4] R. Jeanloz *et al.*, Geophys. J. Int. **62**, 505 (1980).
[5] D. G. Isaak *et al.*, Phys. Rev. B **47**, 7720 (1993).
[6] T. Yagi *et al.*, J. Geophys. Res. **90**, 8784 (1985).
[7] Y. Fei *et al.*, Science **266**, 1678 (1994).
[8] W. M. C. Foulkes *et al.*, Rev. Mod. Phys. **73**, 33 (2001).
[9] L. K. Wagner *et al.*, J. Chem. Phys. **126**, 034105 (2007).
[10] See EPAPS Document No. E-PRLTAO-101-017844 for supplementary information regarding the magnetic moments, equation of state, and pseudopotentials. For more information on EPAPS, see http://www.aip.org/pubservs/epaps.html.
[11] L. Mitáš *et al.*, J. Chem. Phys. **95**, 3467 (1991).
[12] J. Kolorenč *et al.*, Phys. Rev. B **75**, 235118 (2007).
[13] J. P. Perdew *et al.*, J. Chem. Phys. **105**, 9982 (1996).
[14] J. P. Perdew *et al.*, Phys. Rev. Lett. **77**, 3865 (1996).
[15] P. R. C. Kent *et al.*, Phys. Rev. B **57**, 15 293 (1998).
[16] L. Wagner *et al.*, Chem. Phys. Lett. **370**, 412 (2003).
[17] C. Lin *et al.*, Phys. Rev. E **64**, 016702 (2001).
[18] S. Chiesa *et al.*, Phys. Rev. Lett. **97**, 076404 (2006).
[19] *CRC Handbook of Chemistry and Physics*, edited by D. R. Linde (CRC Press, Boca Raton, FL, 2007).
[20] H. K. Bowen *et al.*, J. Solid State Chem. **12**, 355 (1975).
[21] G. D. Jones, Phys. Rev. **155**, 259 (1967).
[22] A. Hjortsberg *et al.*, Phys. Rev. B **37**, 3196 (1988).
[23] C. A. McCammon *et al.*, Phys. Chem. Miner. **10**, 106 (1984).
[24] I. Jackson *et al.*, J. Geophys. Res. **95**, 21 671 (1990).
[25] J. Zhang, Phys. Rev. Lett. **84**, 507 (2000).
[26] H. Mao *et al.*, Phys. Earth Planet. Inter. **96**, 135 (1996).
[27] T. Kondo *et al.*, Phys. Earth Planet. Inter. **143–144**, 201 (2004).
[28] R. L. Clendenen *et al.*, J. Chem. Phys. **44**, 4223 (1966).
[29] L. K. Wagner *et al.*, arXiv:0710.4361; www.qwalk.org.
[30] V. Saunders *et al.*, *CRYSTAL2003 User's Manual* (University of Torino, Torino, 2003).